



In silico study of carvone derivatives as potential neuraminidase inhibitors

Noorakmar Jusoh¹ · Hasanuddin Zainal² · Azzmer Azzar Abdul Hamid² · Noraslinda M. Bunnori² ·
Khairul Bariyyah Abd Halim² · Shafida Abd Hamid¹

Received: 18 May 2017 / Accepted: 11 February 2018 / Published online: 15 March 2018
© Springer-Verlag GmbH Germany, part of Springer Nature 2018

Abstract

Recent outbreaks of highly pathogenic influenza strains have highlighted the need to develop new anti-influenza drugs. Here, we report an in silico study of carvone derivatives to analyze their binding modes with neuraminidase (NA) active sites. Two proposed carvone analogues, **CV(A)** and **CV(B)**, with 36 designed ligands were predicted to inhibit NA (PDB ID: 3TI6) using molecular docking. The design is based on structural resemblance with the commercial inhibitor, oseltamivir (**OTV**), ligand polarity, and amino acid residues in the NA active sites. Docking simulations revealed that ligand **A18** has the lowest energy binding (ΔG_{bind}) value of $-8.30 \text{ kcal mol}^{-1}$, comparable to **OTV** with ΔG_{bind} of $-8.72 \text{ kcal mol}^{-1}$. **A18** formed seven hydrogen bonds (H-bonds) at residues Arg292, Arg371, Asp151, Trp178, Glu227, and Tyr406, while eight H-bonds were formed by **OTV** with amino acids Arg118, Arg292, Arg371, Glu119, Asp151, and Arg152. Molecular dynamics (MD) simulation was conducted to compare the stability between ligand **A18** and **OTV** with NA. Our simulation study showed that the **A18-NA** complex is as stable as the **OTV-NA** complex during the MD simulation of 50 ns through the analysis of RMSD, RMSF, total energy, hydrogen bonding, and MM/PBSA free energy calculations.

Keywords Influenza neuraminidase · Molecular docking · Carvone · MM/PBSA

Introduction

Influenza is an infectious disease that causes significant fatality in the human population. The rapid emergence of several mutant antigens caused the ineffectiveness of vaccines against influenza virus. To date, only three antiviral agents have been approved for the treatment of influenza infection namely, zanamivir, oseltamivir, and peramivir (Fig. 1). However, increasing reports of the resistance of these drugs drive

researchers to explore more effective drugs to combat the virus [1]. Hemagglutinin (HA), neuraminidase (NA), M2 ion channel protein, and endonuclease are several molecular targets identified for drug intervention [2]. Among these potential molecules, NA appears to be an attractive target for drug development [3]. NA is a major glycoprotein that can be found on the virus surface, which catalyzes the cleavage of sialic acid residues from glycolipids and glycoproteins [4]. The protein possesses enzymatic activity that is essential for viral replication and infection.

Research showed that NA is not only crucial in the release of virion, but also needed in the movement of virus through the mucus of the respiratory tract [6]. Therefore, one of the strategies to curb the infection is by inhibiting the NA so that the host immune system has sufficient time to eliminate the virus.

Molecular modeling and structure-based drug design (SBDD) provide great contributions for modern drug development [7]. Docking study revealed that the introduction of amino group substituents to oseltamivir may help to tighten the binding of NA, and thereby decrease the resistance of the enzyme toward the inhibitors [8]. NA has five main conserved

Electronic supplementary material The online version of this article (<https://doi.org/10.1007/s00894-018-3619-6>) contains supplementary material, which is available to authorized users.

✉ Shafida Abd Hamid
shafida@iium.edu.my

¹ Department of Chemistry, Kulliyah of Science, International Islamic University Malaysia, 25200 Bandar Indera Mahkota Kuantan, Pahang, Malaysia

² Department of Biotechnology, Kulliyah of Science, International Islamic University Malaysia, 25200 Bandar Indera Mahkota Kuantan, Pahang, Malaysia

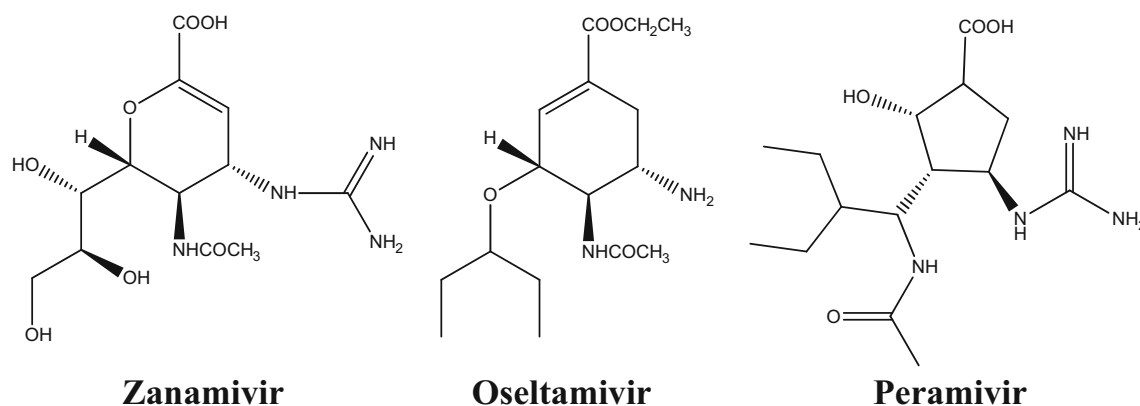


Fig. 1 Chemical structures of neuraminidase inhibitors [5]

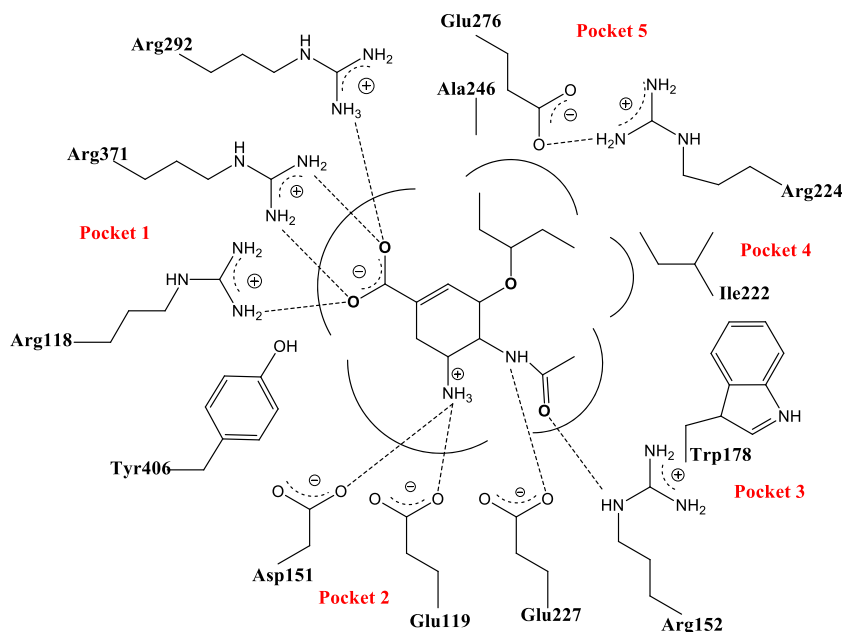
residues of binding sites (Fig. 2) [9]. The positively charged pocket 1, which consists of Arg118, Arg292, and Arg371 interacts with the carboxylate group via hydrogen bonding interaction. The negatively charged pocket 2 comprising Glu119, Glu227, and Asp151 interacts with amino or guanidine group of substrate [10]. In pocket 3, the side chains of Trp178 and Ile222 form hydrophobic interaction while the polar group of Arg152 binds with the oxygen in acetyl substituent. Pocket 4 is primarily a hydrophobic region, derived from side chain Ile222 and the hydrophobic face of Arg224. Pocket 5 is made of a polar Glu276, acting as a hydrogen bond acceptor, and Ala246 to form an additional hydrophobic region [11, 12]. Manipulations of these pockets were extensively done by researchers in designing potential inhibitors that have high binding ability in the neuraminidase active site [6, 13].

Research on NA active sites and structural activity study (SAR) of published NA inhibitors showed that NA inhibition

is mainly determined by the relative position of four substituents (carboxylate, glycerol or hydrophobic side chain, acetamido, and amino or guanidine) of the central ring [11]. Replacing the hydroxyl group of Neu5Ac2en (DANA) with guanidine showed better activity in the NA active site [12]. The inhibitor drug structure, named zanamivir, was then marketed as Relenza. Oseltamivir (Tamiflu®), developed by Kim and his group (2000) consists of all four substituents.

Carvone is a monoterpene ketone, which can be naturally found in spearmint essential oil, *Mentha spicata* [14]. It consists of a cyclohexenone attached to an isopropenyl side chain, which contains an isolated C=C double bond. It occurs as dextrorotatory (*d*-carvone) and levorotatory (*l*-carvone) enantiomers, which are colorless to pale yellow liquids with a characteristic caraway and spearmint odor, respectively. In vitro and in vivo studies revealed that carvone and its derivatives exhibit various biological properties, such as anti-bacterial,

Fig. 2 Structures of oseltamivir complexed in neuraminidase active sites [12]. The five binding pockets were labeled as pocket 1, 2, 3, 4, and 5



anti-fungal, anti-oxidant, anti-tumor, and anti-inflammatory activities [14]. However, no anti-viral activity has been reported using carvone as a core structure. Therefore, this work focuses on the design of the carvone derivatives and studies their binding modes with NA residues through molecular docking and the molecular dynamic simulations approach.

Methods

NA and ligand preparation

The crystal structure of 2009 pandemic H1N1 neuraminidase complexed with oseltamivir (PDB ID: 3TI6) was downloaded from the RCSB Protein Data Bank (<http://www.rcsb.org>). The water and nonprotein molecules were removed, while only the neuraminidase monomer structure was used. The structures of the 36 ligands were drawn and optimized in ChemSketch. All the ligands were designed by modifications at R₁, R₂, and R₃ for both CV(A) and CV(B) (Fig. 3). The modification of compounds is focused on: NH₂ or aliphatic amine at R₁ position, guanidine or acetamide at R₂ position, and ester or aromatic amine at R₃ position.

Molecular docking

We employed AutoDock 4.2 software (available at <http://autodock.scripps.edu>) to perform the molecular docking simulations. The protein was protonated with polar hydrogens and given Kollman charge. The docking runs were set up with a grid volume of 60 points each with the default 0.375 Å. The setting of the grid center was set to -31.016, 13.162, and 23.488 for *x*, *y*, and *z* value, respectively. The binding residues were identified by submitting the PDB ID:3TI6 into the ligand contact tool (LCT) program (<http://firedb.bioinfo.cnio.es/Php/Contact.php>) [15]. This program calculates the contact between the

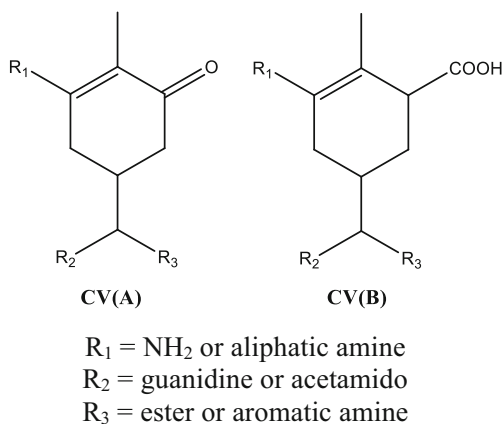


Fig. 3 Design of carvone derivatives

binding residues of NA receptor with oseltamivir using default parameters. The identified binding residues in the active sites were Arg118, Arg292, Arg371, Asp151, Asp152, Trp178, Glu227, Glu277, Arg224, and Tyr406. The docking experiment was performed for 20 genetic algorithm (GA) runs. Docking software supplied with AutoDock 4.0 and AutoGrid 4.0 was used to produce grid maps. The Lamarckian genetic algorithm (LGA) was chosen to improve the energy evaluation in docking. The results were evaluated by analyzing the RMSD values, ligand-protein interactions, energy of binding (ΔG_{bind}) as well as the number of existing conformations in a population cluster. The estimated ΔG_{bind} was calculated as the sum of final intermolecular energy, van der Waals, hydrogen bond and desolvation energies, electrostatic energy, final total internal energy, torsional free energy, and unbound system's energy [16]. The ligand-protein interaction was visualized using Pymol. Subsequently, LIGPLOT tool [17] was performed to explore the intermolecular contacts of hydrogen bonds and hydrophobic interactions in the complex structures.

Molecular dynamics (MD) simulation

MD simulations were performed using the GROMACS 5.1.4 package with the standard GROMOS96 53a6 force field parameters [18]. The system was immersed in a cubic water box and the energy of the complexes was minimized using the steepest descent approach realized in the GROMACS package. The PRODRG server [19] was used to generate ligand topology. An appropriate number of counter ions were added to neutralize the total charge of the system, and 1000 steps of steepest descent energy minimization were carried out for the protein-ligand complex. The system was equilibrated at 300 K after the energy minimization. The water molecules were permitted to relax surrounding the protein, and the relaxation time of water was 50 ps. Finally, the full system was subjected to 50 ns MD simulation at 310 K temperature and 1 bar pressure. The particle mesh Ewald (MPE) method for long-range electrostatics, a 14 Å cut off for van der Waals interactions, a 12 cut off for coulomb interaction with updates every 10 steps, and the Lincs algorithm for covalent bond constraints were used [20]. Root mean square deviation (RMSD), root mean square fluctuation (RMSF), total energy, and H-bonds formed between the residues were analyzed through Gromacs utilities *g_rmsd*, *g_rmsf*, *g_energy*, and *g_hbond*, respectively. The MD runs were carried out in triplicate for each ligand.

MM-PBSA binding free energy calculation

Combined with MD simulation, binding free energy calculation methods have become powerful tools in providing quantitative measurement for protein-ligand interactions [21]. In this study, a Gromacs tool named *g_mmpbsa* was used to calculate the binding free energy of protein-ligand complexes

from MD trajectories [22]. This tool implements the MM-PBSA approach by using subroutines derived from Gromacs and Adaptive Poisson-Boltzmann Solver packages without run-time dependency on external software, and is suitable for binding energy calculations on molecular systems because its performance is comparable to the AMBER package. Of note, *g_mmpbsa* only calculates the electrostatic and van der Waals components of gas-phase energy, as the bonded contribution is by definition zero in the single-trajectory approach. Besides, the entropy term is not evaluated yet, as it has become common practice in recent works to exclude the entropy term from the MM-PBSA calculation. Therefore, binding energy is calculated as follows:

$$\Delta G_{\text{bind}} = \Delta E_{\text{MM}} + \Delta G_{\text{polar}} + \Delta G_{\text{nonpolar}} \quad (1)$$

where ΔE_{MM} represents the gas-phase energy consisting of electrostatic and van der Waals interaction, ΔG_{polar} denotes polar solvation energy, and $\Delta G_{\text{nonpolar}}$ is nonpolar solvation energy. Subsequently, the energy components ΔE_{MM} , ΔG_{polar} , and $\Delta G_{\text{nonpolar}}$ of each complex were calculated for 11 snapshots extracted every 0.2 ns from the production trajectory from 8 to 10 ns. Other parameters used by *g_mmpbsa* for the free-energy calculation were set based on those described in the developer's publication [22].

Results and discussion

Docking studies

Molecular docking was performed to analyze the SAR of different substituents of the ligands with the NA residues. Three criteria determine the ligand-complex binding affinity, which are energy binding (ΔG_{bind}), inhibition constant (K_i), and hydrogen bond. The more negative the ΔG_{bind} value and the more hydrogen bonds formed, the stronger complex stability between ligand and protein. In this study, the best ligand-protein complex was the lowest ΔG_{bind} value and inhibition constant. Inhibition constant (K_i) is the concentration required by the ligand to inhibit the target protein [23]. Hence, a smaller value of K_i is needed for stronger interaction complex. The negative sign in the binding energy value shows the possibility of spontaneous interaction between ligand and receptor [24]. The estimated ΔG_{bind} was calculated as the sum of final intermolecular energy, van der Waals, hydrogen bond and desolvation energies, electrostatic energy, final total internal energy, torsional free energy, and unbound system's energy [16].

$$\begin{aligned} \Delta G_{\text{bind}} = & \Delta G_{\text{vdw}} + \Delta G_{\text{Hbond}} + \Delta G_{\text{elect}} + \Delta G_{\text{conform}} \\ & + \Delta G_{\text{tor}} + \Delta G_{\text{sol}} \end{aligned}$$

Table 1 shows the energy of binding (ΔG_{bind}) and inhibition constant (K_i) of designed carvone derivatives calculated using AutoDock. The values of ΔG_{bind} and K_i correspond with the thermodynamics Eq. [25].

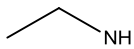
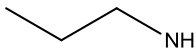
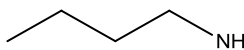
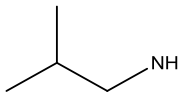
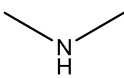
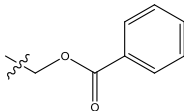
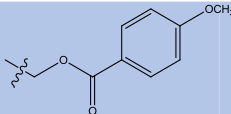
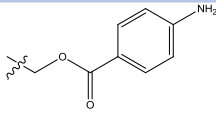
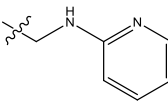
$$\begin{aligned} G^\circ &= -RT \ln K_A \\ K_A &= K_i^{-1} = \frac{[EI]}{[E][I]} \end{aligned}$$

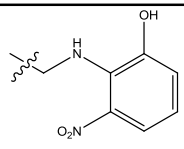
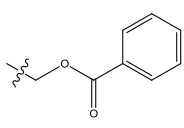
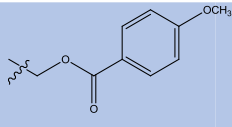
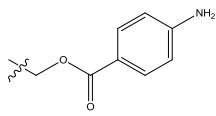
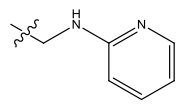
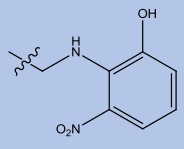
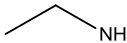
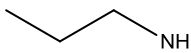
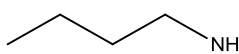
The result shows that the lower the energy binding, the lower the inhibition constant. **A18** has the lowest energy binding ($-8.30 \text{ kcal mol}^{-1}$) and lowest inhibition constant at $0.82 \text{ } \mu\text{M}$. Introducing **A18** with NH_2 at R_1 , guanidine at R_2 , and heterocyclic amine at R_3 position increased the binding affinity toward NA, which is far more favorable compared to its parent compound, **CV** ($-4.77 \text{ kcal mol}^{-1}$). The OH group plays an important role since it formed H-bonds with three residues; Arg292, Arg371, and Tyr406. Oseltamivir (**OTV**) has a ΔG_{bind} of $-8.72 \text{ kcal mol}^{-1}$ with a K_i value of $0.35 \text{ } \mu\text{M}$.

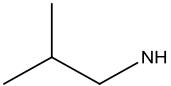
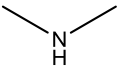
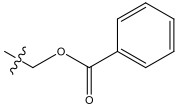
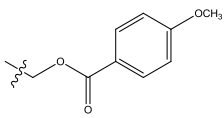
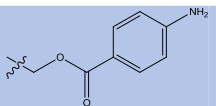
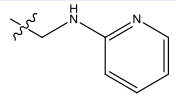
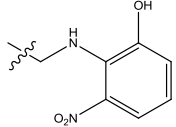
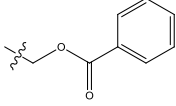
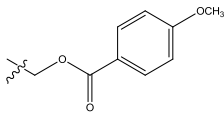
For visualization, PyMol software was used to view the H-bond interaction between the protein-ligand complex and NA active sites (Fig. 4). The figure shows five potential ligands, **A18**, **B18**, **B10**, **A9**, and **A15**, together with **OTV**, which have lower energy binding value of -8.30 , -8.11 , -8.00 , -7.83 , -7.68 , and $-8.72 \text{ kcal mol}^{-1}$, respectively. **OTV** formed eight H-bonds with Arg118, Arg292, Arg371, Glu119, Asp151, and Arg152 residues. Amino acid residues Arg292 and Arg371 formed more than one H-bond, with two H-bonds formed by each residue. This finding is supported by a previous study, which stated that the carboxylic group of oseltamivir had strong interaction in pocket 1 (Arg118, Arg292, and Arg371) [12]. The guanidine group of ligands **A18**, **B10**, and **A15** interact with amino acid residues Asp151, Glu227, and Trp178. The stability of protein-ligands complex is based on the formation of hydrogen bonds. This is because the hydrogen bond could affect the physical-chemical properties, such as melting point, boiling point, and water solubility of compounds. **A18** formed the highest number of H-bonds among all the ligands investigated, indicating that it is the most stable complex during substrate recognition. Thus, **A18** will be further studied for dynamics simulation to analyze their binding stability throughout the simulation.

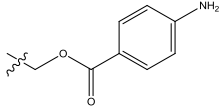
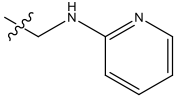
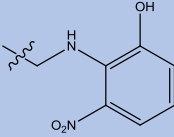
In order to understand the binding modes and structural characteristics, we analyzed the intermolecular contacts in the protein-ligand complex using LIGPLOT tool [17]. LIGPLOT is a program to plot schematic diagrams of protein-ligand interactions, including hydrogen bonds and hydrophobic contacts. Hydrogen bonds are represented by dashed lines between the atoms involved, while hydrophobic contacts are indicated by an arc with spokes radiating toward the ligand atoms they contact (Fig. 5). Figure 5a shows that oxygen atoms of **OTV** are involved in hydrogen bonding with

Table 1 Binding energy (ΔG_{bind}) and inhibition constant, K_i of designed carvone derivatives

Ligands	R ₁	R ₂	R ₃	Free Energy Binding (kcal/mol)	Inhibition constant, K_i (μM)
CV	CH ₃	=CH ₂	CH ₃	-4.77	200.98
A1	NH ₂	=CH ₂	CH ₃	-5.09	185.67
A2		=CH ₂	CH ₃	-5.05	198.66
A3		=CH ₂	CH ₃	-5.26	139.70
A4		=CH ₂	CH ₃	-6.93	8.38
A5		=CH ₂	CH ₃	-5.73	63.27
A6		=CH ₂	CH ₃	-4.70	359.04
A7	NH ₂	NHC=OCH ₃	CH ₃	-6.18	29.42
A8	NH ₂	NHC=OCH ₃		-7.09	13.95
A9	NH₂	NHC=OCH₃		-7.83	1.81
A10	NH ₂	NHC=OCH ₃		-7.47	3.33
A11	NH ₂	NHC=OCH ₃		-6.33	23.08

A12	NH ₂	NHC=OCH ₃		-7.08	6.46
A13	NH ₂	NHC=NHNH ₂	CH ₃	-6.52	16.57
A14	NH ₂	NHC=NHNH ₂		-7.28	4.60
A15	NH₂	NHC=NHNH₂		-7.68	2.35
A16	NH ₂	NHC=NHNH ₂		-7.10	6.19
A17	NH ₂	NHC=NHNH ₂		-6.76	11.16
A18	NH₂	NHC=NHNH₂		-8.30	0.82
B1	NH ₂	=CH ₂	CH ₃	-5.14	170.72
B2		=CH ₂	CH ₃	-4.07	1040
B3		=CH ₂	CH ₃	-6.91	8.66
B4		=CH ₂	CH ₃	-6.85	9.51

B5		=CH ₂	CH ₃	-5.86	50.58
B6		=CH ₂	CH ₃	-5.15	167.82
B7	NH ₂	NHC=OCH ₃	CH ₃	-4.81	297
B8	NH ₂	NHC=OCH ₃		-7.12	5.99
B9	NH ₂	NHC=OCH ₃		-6.05	36.59
B10	NH₂	NHC=OCH₃		-8.00	1.38
B11	NH ₂	NHC=OCH ₃		-4.97	228.27
B12	NH ₂	NHC=OCH ₃		-6.94	8.22
B13	NH ₂	NHC=NHNH ₂	CH ₃	-5.30	130.14
B14	NH ₂	NHC=NHNH ₂		-7.62	2.59
B15	NH ₂	NHC=NHNH ₂		-6.19	29.05

B16	NH ₂	NHC=NHNH ₂		-7.61	2.64
B17	NH ₂	NHC=NHNH ₂		-5.30	129.99
B18	NH₂	NHC=NHNH₂		-8.11	1.15
OTV				-8.72	0.35

The top five ligands with the best Autodock score are highlighted

residues Arg118, Arg292, and Arg371, while oxygen atoms of **A18** formed four hydrogen bondings with Arg292, Arg371, and Tyr406. Two or more arginine residues surrounding the carboxylic group of NA inhibitors play a vital role in stabilizing the complex structures [26]. Hydrophobic contacts also play a key role in the stability of the ligand and protein interaction. Eight and seven hydrophobic bonds were formed surrounding **OTV-NA** and **A18-NA** complex, respectively; thus, indicating that both complex are stable.

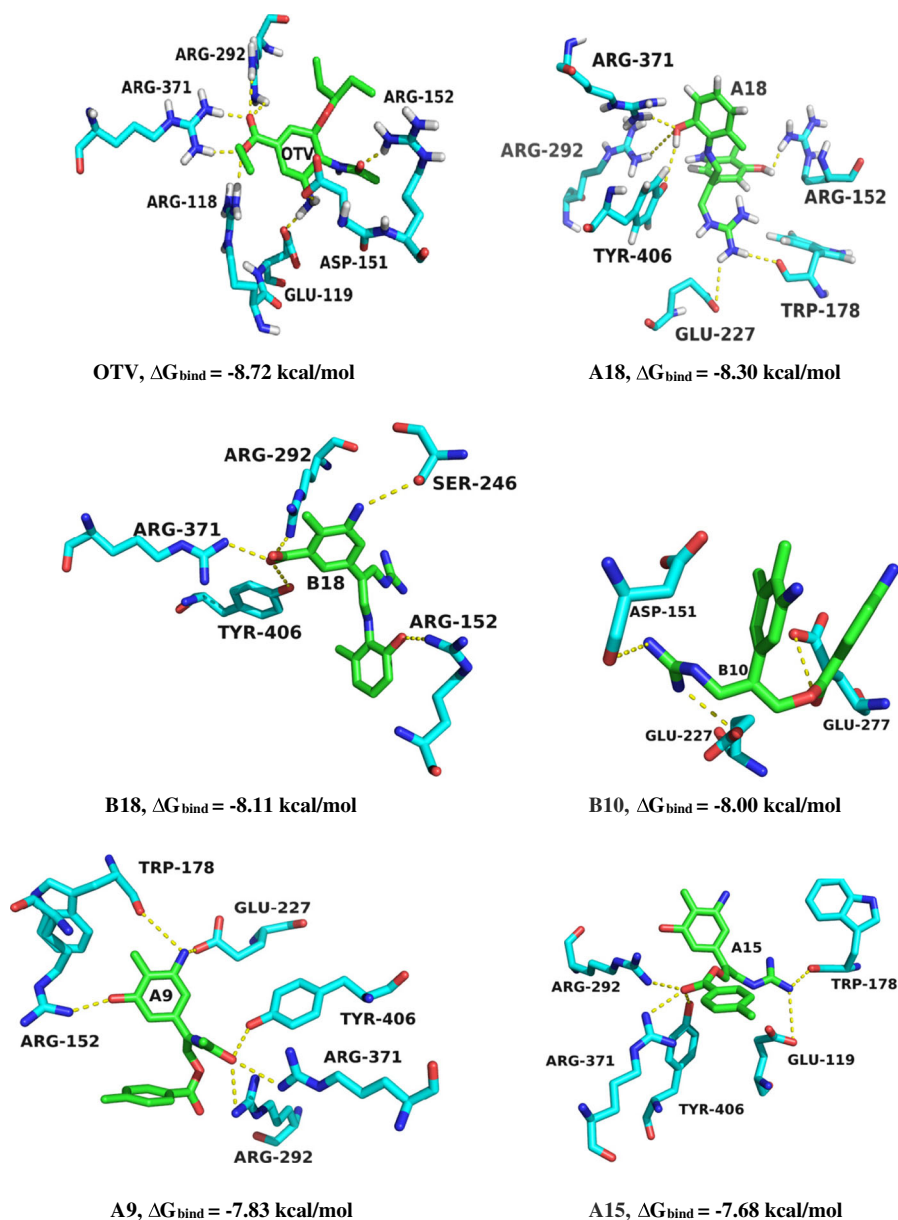
Molecular dynamics simulation

Molecular dynamics simulation was performed to compare the binding stability between **A18** and oseltamivir (**OTV**) with NA. **A18** was chosen as it has the lowest binding energy among 36 ligands, comparable to **OTV**, with ΔG_{bind} of $-8.30 \text{ kcal mol}^{-1}$ and $-8.72 \text{ kcal mol}^{-1}$, respectively. RMSD analysis provides an overall picture of how much the three-dimensional structure of the proteins fluctuates and changes conformation over the simulation time. Here, the RMSD value of the protein backbone was examined to investigate the stability of the protein in the system. Figure 6a shows the average of backbone RMSD values of **A18-NA** and **OTV-NA** complex

structure throughout the 50 ns simulation. The figure indicates that both complexes were stable during the MD simulation. **OTV-NA** complex showed RMSD fluctuations at $\sim 1\text{--}3 \text{ \AA}$ from 0 until 20 ns, while for **A18-NA** complex it fluctuated at $\sim 2\text{--}2.5 \text{ \AA}$ from 5 ns until the end of the simulation. The **A18-NA** complex has lower RMSD values compared to **OTV** complex, indicating that **A18** is more stable than **OTV-NA**. Furthermore, we analyzed the RMSD profile of the active site residues as well as the ligand in protein-ligand. The RMSD analysis suggested that both ligands achieved stable confirmation after simulations (Fig. 6b and c). The root mean square fluctuations (RMSF) value of both complexes was also examined to analyze the fluctuations of each residue in NA protein (Fig. 6d). The figure shows the fluctuations of the residues from 82 to 469. These residue fluctuations of NA proteins denote the binding ability of these proteins with each ligand. From this RMSF analysis, we can conclude that both complexes of **A18** and **OTV** show a similar pattern of RMSF values, ranged between 0.5 \AA and 5 \AA .

The plots for the variation of the total energy for system was also analyzed in MD simulation, as indicated in Fig. 7(a). The graph shows that the total energy for the system remained

Fig. 4 Docking poses showed the H-bonds formed (yellow dashed line) between five potential carvedone derivatives and the commercial inhibitor, OTV, with the NA active site. The figures were generated using PyMol



constant throughout the simulation with the energy value at -6.4×10^5 kcal mol⁻¹. The stability of protein-ligand complex was further assessed by the analysis of hydrogen bonding interactions throughout the MD simulation. Hydrogen bonding is one of the main factors maintaining the binding between the ligand and acceptor. A donor and an acceptor atom form hydrogen bonds when the distance between them is less than 3.5 Å [27]. The number of hydrogen bonds between **OTV-NA** complex and **A18-NA** complex across simulation can be seen in Fig. 7(b). The analysis suggests that **OTV-NA** complex (blue) formed three H-bonds, whereas in **A18-NA** complex (red), only two H-bonds were observed throughout the simulation. Even though only a few hydrogens were observed for **A18**, the interactions may be stabilized by hydrophobic

contacts. Weak intermolecular interactions like hydrophobic and hydrogen bonds may play an important role in stabilizing a ligand at the interface of a protein structure [28].

The details of H-bonds formation before and after MD simulation can be seen in Fig. 8. Pre-MD simulation of **OTV** formed various hydrogen bonds with protein residues namely Arg371, Arg292, Glu119, Asp151, Arg152 (Fig. 8a). Post-MD simulation of **OTV** was found to form hydrogen bonds with Arg371, Arg227, and Arg277 (Fig. 8b). Four hydrogen bonds with Arg292, Glu119, Asp151, and Arg152 were lost during simulations; however, two new hydrogen bonds were formed with residues Arg227 and Arg277. For **A18**, a difference can also be observed before and after MD simulation.

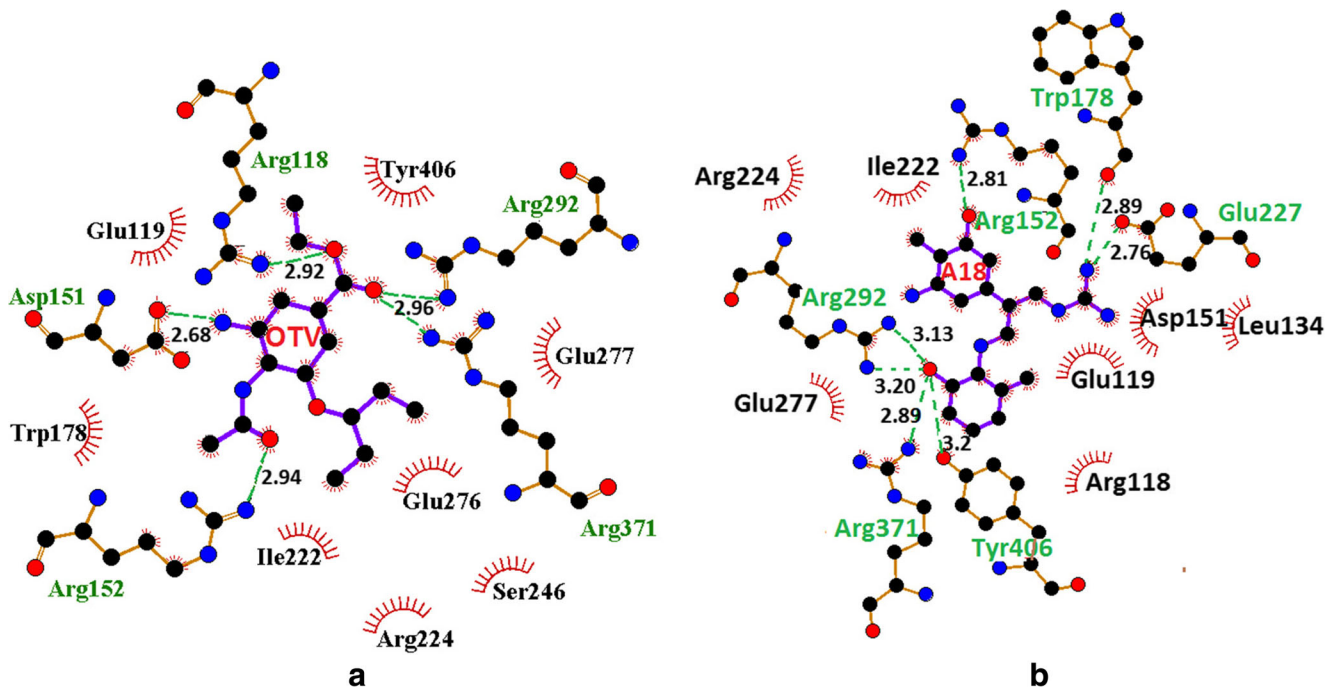


Fig. 5 Hydrogen and hydrophobic interaction of OTV (a) and A18 (b) with amino acid residues

Fig. 6 RMSD value of protein backbone (a); RMSD value of NA residue (b); RMSD of ligand (c) and RMSF value (d) of A18 and OTV complex throughout 50 ns MD simulation

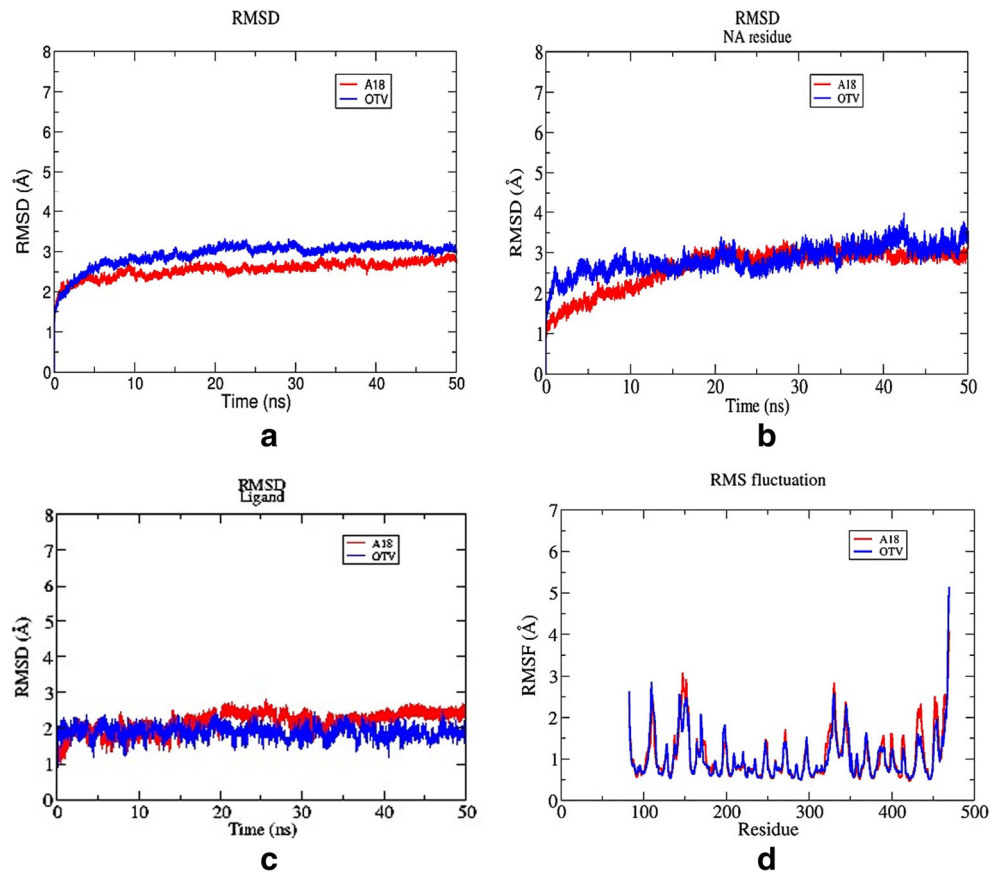
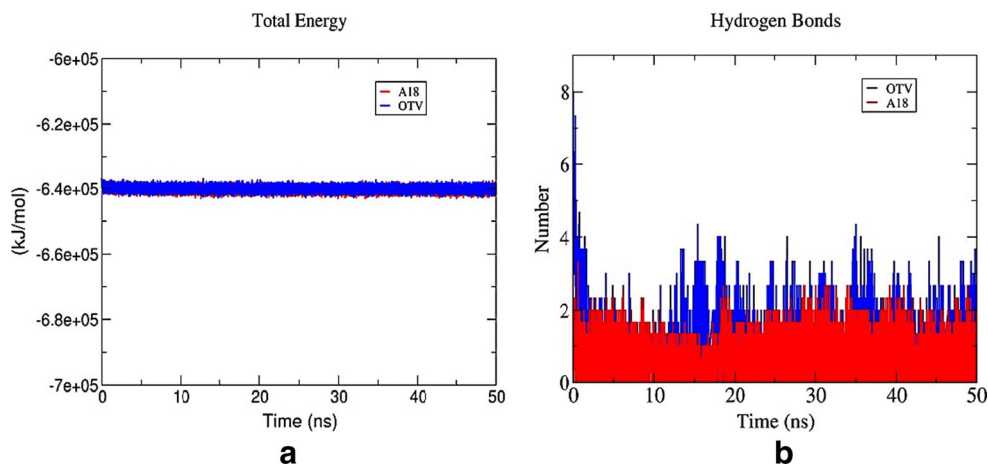


Fig. 7 The total energy (a) and the number of H-bonds (b) observed between the ligand-protein complex from a representative of OTV and A18 simulations



Post-MD simulation of **A18** showed it formed hydrogen bonds with two residues Arg152 and Arg156 (Fig. 8d). Here, we can conclude that both ligands interacted with NA active site residues by hydrogen bonds as well as hydrophobic interactions that further stabilized the protein-ligand complex.

MM-PBSA analysis

The binding free energies for the two complexes **OTV** and **A18** were estimated using the MM-PBSA method to find

the binding affinity of the ligands. The binding free energy includes various components of interaction energy, such as van der Waals, electrostatic, polar solvation, and nonpolar solvation energy. The calculated binding free energies (Table 2) were -30.398 ± 4.25 kcal mol⁻¹ and -96.644 ± 2.34 kcal mol⁻¹ for **OTV** and **A18**, respectively, indicating that **A18** possessed higher negative binding free energy value compared to **OTV**. In terms of components making up binding energy, van der Waals energy, electrostatic energy, and non-polar energy negatively contributed to the total interaction energy, whereas polar solvation energy positively contributed

Fig. 8 Hydrogen bond interactions (yellow dashed line) observed between the ligand-protein complex before and after MD simulation (a) and (c) OTV-NA complex; (b) and (d) A18-NA complex throughout 50 ns MD simulation

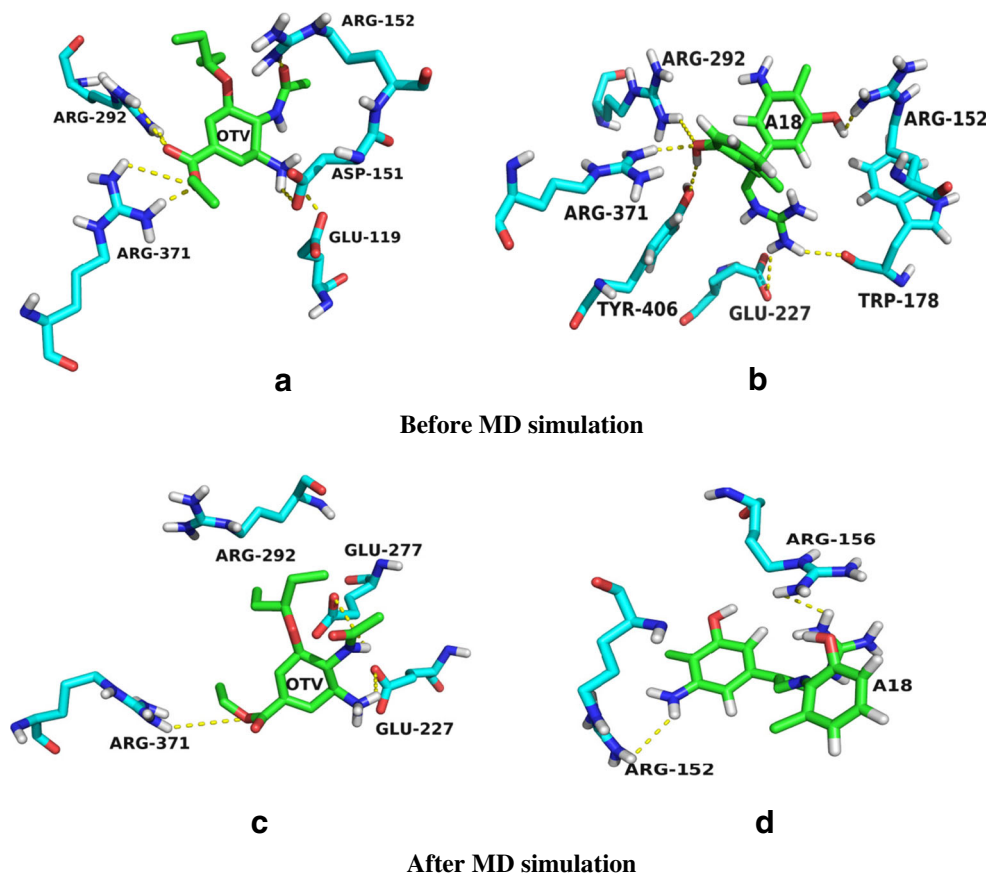


Table 2 Binding free energies (kcal mol⁻¹) resulting from MM-PBSA analysis of the OTV-NA and A18-NA complexes

	ΔE_{vdw}	ΔE_{elec}	ΔG_{polar}	$\Delta G_{\text{nonpolar}}$	ΔG_{bind}
OTV	-107.361 ± 2.20	-435.944 ± 4.44	526.758 ± 7.07	-13.784 ± 0.21	-30.398 ± 4.25
A18	-142.282 ± 1.95	-14.829 ± 1.43	75.265 ± 2.59	-14.903 ± 0.23	-96.644 ± 2.34

to total free binding energy. Moreover, van der Waals interaction gives a much larger contribution than electrostatic interactions for **A18**.

Conclusions

Molecular docking and the molecular dynamics approach were used to investigate the binding activity of 36 designed carvone derivatives toward neuraminidase active sites. Our docking study indicates that all the ligands showed strong binding affinity against active sites of NA, ranging from -4.77 to -8.30 kcal mol⁻¹. Among the 36 ligands, **A18** has the lowest binding energy of -8.30 kcal mol⁻¹ with seven H-bonds formed in the amino acid residues Arg292, Arg371, Asp151, Trp178, and Glu227, comparable with the commercial inhibitor, oseltamivir (**OTV**). The amino and acetamido groups mainly contributed to the binding affinity of the **A18** binding toward NA active sites. Our simulation result suggests that the **A18-NA** complex was stable during the MD simulation. Although the average H-bond number was lower than **OTV**, the H-bonds formed between **A18** and NA active site residues Arg152 and Arg156 were stable throughout the 50 ns simulations. Hence, this in silico study reveals that carvone derivatives could serve as potent neuraminidase inhibitors against influenza virus.

Acknowledgments SAH thanks Malaysia Ministry of Higher Education (MOHE) for Fundamental Research Grant Scheme (FRGS14-098-0339) and myBrain15 scholarship for NJ.

References

- Samson M, Pizzomo A, Abed Y, Boivin G (2013) Influenza virus resistance to neuraminidase inhibitors. *Antivir Res* 98(2):174–185
- Wang GT, Chen Y, Wang S, Gentles R, Sowin T, Kati W, Muchmore S, Giranda V, Stewart K, Sham H, Kempf D, Laver WG (2001) Design, Synthesis, and Structural Analysis of Influenza Neuraminidase Inhibitors Containing Pyrrolidine Cores. *Lett Org Chem* 167:1192–1201
- John P, Adabala P, Legresley EB, Bance N, Niikura M, Pinto BM (2013) Exploitation of the catalytic site and 150 cavity for Design of influenza neuraminidase inhibitors. *J Org Chem* 78:10867–10877
- von Itzstein M (2007) The war against influenza: discovery and development of sialidase inhibitors. *Nat. Rev. Drug Discov.* 6: 967–974
- von Itzstein M, Wu W-Y, Kok GB, Pegg MS, Dyason JC, Jin B, Van Phan T, Smythe ML, White HF, Oliver SW, Colman PM, Varghese JN, Ryan DM, Woods JM, Bethell RC, Hotham VJ, Cameron JM, Penn CR (1993) Rational design of potent sialidase-based inhibitors of influenza virus replication. *Nature* 363:418–423
- Gong J, Xu W, Zhang J (2007) Structure and functions of influenza virus neuraminidase. *Curr Med Chem* 14(1):113–122
- Pranita SSK, Kore P, Mutha MM, Antre RV, Oswal RJ (2012) Computer-aided drug design: an innovative tool for modeling. *Open J Med Chem* 2(1):139–148
- D'Souza C, Kanyalkar M, Joshi M, Coutinho E, Srivastava S (2009) Probing molecular level interaction of oseltamivir with H5N1-NA and model membranes by molecular docking, multinuclear NMR and DSC methods. *Biochim Biophys Acta Biomembr.* 1788(2):484–494
- Stoll V, Stewart KD, Maring CJ, Muchmore S, Giranda V, Gui Y, Gu Y, Wang G, Chen Y, Sun M, Zhao C, Kennedy AL, Madigan DL, Xu Y, Saldivar A, Kati W, Laver G, Sowin T, Sham HL, Greer J, Kempf D (2003) Influenza neuraminidase inhibitors: structure-based design of a novel inhibitor series. *Biochemistry* 42(3):718–727
- Ye D, Shin W-J, Li N, Tang W, Feng E, Li J, He P-L, Zuo J-P, Kim H, Nam K-Y, Zhu W, Seong B-L, No KT, Jiang H, Liu H (2012) Synthesis of C-4-modified zanamivir analogs as neuraminidase inhibitors and their anti-AIV activities. *Eur J Med Chem* 54:764–770
- Rudrawar S, Dyason JC, Rameix-Welti MA, Rose FJ, Kerry PS, Russell RJ, van der Werf S, Thomson RJ, Naffakh N, von Itzstein M (2010) Novel sialic acid derivatives lock open the 150-loop of an influenza A virus group-1 sialidase. *Nat Commun* 1:113–117
- von Itzstein M, Thomson R (2009) Anti-influenza drugs: the development of sialidase inhibitors. *Handb Exp Pharmacol* 189:111–154
- Lew W, Chen X, Kim CU (2000) Discovery and development of GS 4104 (oseltamivir): an orally active influenza neuraminidase inhibitor. *Curr Med Chem* 7(6):663–672
- Decarvalho C, Dafonseca M (2006) Carvone: why and how should one bother to produce this terpene. *Food Chem* 95(3):413–422
- López G, Valencia A, Tress ML (2007) Firestar-prediction of functionally important residues using structural templates and alignment reliability. *Nucleic Acids Res* 35(Suppl2):573–577
- Hariono M, Abdullah N, Damodaran KV, Kamarulzaman EE (2016) Potential new H1N1 neuraminidase inhibitors from ferulic acid and vanillin: molecular modelling, synthesis and in vitro assay. *Nat Publ Gr* <https://doi.org/10.1038/srep38692>
- Wallace AC, Laskowski RA, Thornton JM (1995) LIGPLOT: a program to generate schematic diagrams of protein-ligand interactions clean up structure. *Protein Eng* 8(2):127–134
- Van Gunsteren FW, Billeter SR, Eising AA, Hünenberger PH, Krüger P, Mark AE, Scott WRP, Tironi IG (1996) Biomolecular simulation: the GROMOS96 manual and user guide. Vdf Hochschulverlag AG an der ETH Zürich, Zürich
- Schüttelkopf AW, Van Aalten DMF (2004) PRODRG: a tool for high-throughput crystallography of protein-ligand complexes. *Acta Crystallogr D Biol Crystallogr* 60(8):1355–1363
- Asadollahi-Baboli M, Mani-Varnosfaderani A (2013) Molecular docking, molecular dynamics simulation, and QSAR model on

- potent thiazolidine-4-carboxylic acid inhibitors of influenza neuraminidase. *Med Chem Res* 22(4):1700–1710
21. He JY, Li C, Wu G (2014) Discovery of potential drugs for human-infecting H7N9 virus containing R294K mutation. *Drug Des Devel Ther* 8:2377–2390
 22. Kumari R, Kumar R, Lynn A (2014) G-mmpbsa -a GROMACS tool for high-throughput MM-PBSA calculations. *J Chem Inf Model* 54(7):1951–1962
 23. Morris G, Goodsell D (1998) Automated docking using a Lamarckian genetic algorithm and an empirical binding free energy function. *J Comput Chem* 19:1639–1662
 24. Morris GM, Huey R, Olson AJ (2008) UNIT using AutoDock for ligand-receptor docking. *Curr Protocols Bioinform*. <https://doi.org/10.1002/0471250953.bi0814s24>
 25. Kang JW, Hwang HJ, Song KO, Choi WY, Byun KR, Kwon OK, Lee JH, Kim WW, Muchtaridi M, Aliyudin A, Holik HA (2003) Potential activity of some natural products compounds as neuraminidase inhibitors based on molecular docking simulation and in vitro test. *J Korean Phys Soc* 5(3):65–73
 26. Wang T, Wade RC (2001) Comparative binding energy (COMBINE) analysis of influenza neuraminidase-inhibitor complexes. *J Med Chem* 44:961–971
 27. Liu Z, Zhao J, Li W, Wang X, Xu J, Xie J, Tao K, Shen L, Zhang R (2015) Molecular docking of potential inhibitors for influenza H7N9. *Comput Math Methods Med*. 2015:1–9
 28. Patil R, Das S, Stanley A, Yadav L, Sudhakar A (2010) Optimized hydrophobic interactions and hydrogen bonding at the target-ligand interface leads the pathways of drug-designing. *PLoS One* 5(8): e12029